Vacuum 158 (2018) 121–125

Contents lists available at ScienceDirect

Vacuum

journal homepage: www.elsevier.com/locate/vacuum

Short communication

Ageing response of an Al-Mg-Mn-Sc-Zr alloy processed by laser metal deposition in thin-wall structures

Tong Zhao[a,*], Wangcan Cai[a], Marius Dahmen[b], Jonathan Schaible[b], Chen Hong[b], Andres Gasser[a,b], Andreas Weisheit[a,b], Tim Biermann[a], Ingomar Kelbassa[c], Han Zhang[d,e], Dongdong Gu[d,e], Johannes Henrich Schleifenbaum[b,f]

[a] *RWTH Aachen University LLT - Chair for Laser Technology, Steinbachstraße 15, D-52074, Aachen, Germany*
[b] *Fraunhofer ILT - Institute for Laser Technology, Steinbachstraße 15, D-52074, Aachen, Germany*
[c] *Siemens AG Power and Gas, Huttenstraße 12, D-10553, Berlin, Germany*
[d] *College of Materials Science and Technology, Nanjing University of Aeronautics and Astronautics, Yudao Street 29, Nanjing, 210016, PR China*
[e] *Jiangsu Provincial Engineering Laboratory for Laser Additive Manufacturing of High-Performance Metallic Components, Yudao Street 29, Nanjing 210016, PR China*
[f] *RWTH Aachen University DAP - Digital Additive Production, Steinbachstraße 15, D-52074, Aachen, Germany*

ARTICLE INFO

Keywords:
Additive manufacturing
Aluminium scandium alloys
Precipitation
Mushy state
Thermal history
Grain refinement

ABSTRACT

The use of aluminium alloys containing Sc and Zr in additive manufacturing (AM) provides new solutions for lightweight design. Representative thin-wall structured parts were additively fabricated with a commercially available Al-4.55Mg-0.51Mn-0.65Sc-0.30Zr alloy in Laser Metal Deposition (LMD) process. A bi-directional and a uni-directional scan strategy were applied and laser power from 500 W to 600 W was used. Nanohardness tests were conducted on specimens aged at 300 °C for up to 19 h to observe the ageing responses. Fine-grained microstructures with few micro-sized precipitates containing Sc- and Zr were found in the last track of every specimen. The area formed by the track-overlapping was the opposite, but an apparent hardening was observed only after the ageing. AM-processes with local remelting are facing the challenge to exert the potential strengthening effect of aluminium alloys containing Sc. The mushy state must be suppressed to prevent the waste of the expensive rare elements.

Aluminium alloys containing Sc and Zr are promising materials for the next generation of lightweight constructions due to the potent precipitation hardening and the ability to form fine-grained microstructures. Earlier studies have demonstrated a significant grain refinement due to the simplified nucleation of the matrix caused by the preformed Al_3Sc precipitates in Al-Sc alloys with hypereutectic ($>$ 0.55 wt.% Sc) scandium contents [1–3]. It has been pointed out that both the precipitate number density and the coarsening resistance can be further improved by adding zirconium to Al-Sc-alloys [4]. Zirconium, like scandium, can also be separately added into aluminium alloys to help avoid hot tearing defects through formation of fine-grained equiaxed microstructures [5,6]. However, micro alloying makes a meaningful difference to the mechanical properties in conjunction with a properly arranged and process-dependent thermal history, which is determined by the process condition as well as the subsequent heat treatment [7], the mechanical treatment [8], and by the delivered state of the materials [9].

Laser Metal Deposition (LMD, also termed as Direct Metal Depsition) as a mainstream additive manufacturing (AM) process is characterized by powder being fed through a moveable nozzle and is thus suitable for adding structures to given large-scale parts [10]. Metal powders are fed into a molten pool that is induced by laser heating and shielded by inert gas. Because materials in metallic AM are repeatedly heated during the building process, controlling the as-processed ageing condition of age-hardenable materials, just like aluminium alloys containing Sc and Zr, is still not possible [11,12]. In aluminium alloys containing Sc and Zr, solid solution strengthening, grain boundary strengthening and precipitation strengthening are suggested to be the main strengthening mechanisms [9]. However, the contribution of a certain mechanism depends on the specific processing conditions. Due to the limited equilibrium solubility of Sc in the aluminium-matrix, a high number density of obstacles for dislocation movement of the precipitation hardening [13] cannot be achieved through a conventional solid-solution heat treatment below the solidus [14] but from a supersaturated state left by the fastest possible cooling of the molten metal [9]. A high supersaturation ensures the driving force for the

---

[*] Corresponding author.
E-mail address: tong.zhao@llt.rwth-aachen.de (T. Zhao).

https://doi.org/10.1016/j.vacuum.2018.09.052
Received 30 May 2018; Received in revised form 28 July 2018; Accepted 25 September 2018

precipitation of nano-sized coherent $Al_3(Sc,Zr)$ precipitates whose number density can be increased by raising the ageing temperature [13]. However the temperature should not exceed the upper limit, for example, as suggested that dispersed distributed coherence $Al_3(Sc,Zr)$ phases in Al-0.2Sc (wt.%) alloy are only formed through a continuous transformation after the ageing at about 310 °C rather than 410 °C or even higher [15]. In this regard, electro-beam based processes are shown to effectively produce highly supersaturated resolidified molten pools in localized remelted Al-Sc-alloy substrates with a significant improved age-hardening potential [13,16,17]. However, in AM the heating and cooling condition as well as the microstructure will be evolutionarily changed during the metal deposition of solid bodies [18,19]. The thermal history is thus more complex than in the case of direct substrate remelting, which was examined in the previous studies that used electro-beam processes.

As for AM of aluminium alloys containing Sc and Zr, studies have mostly been carried out in Laser Powder-Bed Fusion (LPBF, also termed as Selective Laser Melting) [7,20–26] where fine- and coarse-grained bimodal microstructures have been observed within the overlapping zones between tracks. Due to the limited working space of the powder bed or the vacuum chamber, neither LPBF nor electro-beam AM processes are not suitable for processing large-sized parts. As for the rarely reported LMD of Al-Sc alloys, the thermal history issue has been preliminarily studied with macroindentation test (HV_5) in a centimeter-scaled area and it was found that the as-processed condition nearly matches the fully aged state [27]. The achievable cooling rate in LMD is considered to be significantly lower than in LPBF, so that the as-casted hardness and the tensile strength achievable in LMD are observed to be two-thirds of those in LPBF [28]. Considering that in AM processes the track overlapping varies across space and time, the thermal history within one part is still difficult to be universally described.

Since an LMD-part merely consists of overlapping welded tracks, the present research is focused on the behaviour of basic thin-wall structures, in which each track was welded on top of the previous, and aims at discussing the ageing response of aluminium alloys containing Sc and Zr processed by powder-feed LMD.

The experiments were performed with a Sc- and Zr-modified Al-Mg-Mn alloy which has a composition of Al-4.55Mg-0.51Mn-0.65Sc-0.30Zr-(0.16Si-0.14Fe-0.04O-(≤ 0.02Zn, Cu, V, Ti)) (wt.%). The material was gas-atomized with 10%, 50% and 90% of the diameters of the powders being less than 23.33 μm, 42.72 μm and 57.68 μm, respectively. The powders were conveyed by compressed argon and fed through a moveable nozzle (Fraunhofer ILT, COAX40) with a conical powder stream (0.18 g/min, spot diameter 0.6 mm). The laser beam (Trumpf HL3006D; spot diameter (86% energy) 1.27 mm; wavelength 1.06 μm; cw-mode) was in coaxial alignment with the powder stream. Two scan strategies were used: two consecutive tracks were welded either bi-directionally without a break time or uni-directionally with a break time of 27 s. The scan speed was 550 mm/min. Three laser power levels of 500 W, 550 W and 600 W were used, so that the laser power was sufficient to generate a molten pool but low enough to not cause any defects like clogging in the nozzle due to melting of powders directly inside the nozzle by the reflected laser beam. Each thin wall (approx. 2.5 mm high) was deposited onto a water-cooled substrate (EN AW-5083, 17.6 °C) and was made of 30 tracks (40 mm long) stacked of top of one another. The vertical offset of the nozzle for each track was 0.1 mm. The experiment setup is shown in Fig. 1.

The differently processed specimens were artificially aged in a heat treatment furnace (Ar-atmosphere) at 300 °C for a duration of 1 h, 3 h, 6 h, 11 h, or 19 h, and then air-cooled (approx. 20 °C/min), or just stored at room temperature (0 h artificial ageing). For analysing, the specimens were cut down in the middle perpendicular to the scan direction. The cross-sectional samples were then cold embedded and metallographically prepared (grinding, polishing with 1 μm diamond suspension) for an indentation hardness test (150 points with 10 mN load, PICODENTOR HM500) along every symmetry axis and scanning electron microscope observations (backscattered electron (BSE) mode, FEI XL30 FEG; Energy-dispersive X-ray spectroscopy (EDX), Leo 1455 EP). For observations using a light optical microscope (LOM, Zeiss Axiophot), the samples were etched with a 10% NaOH solution to observe the molten pool boundaries and were electrolytically etched with Barker's reagent to observe the microstructure.

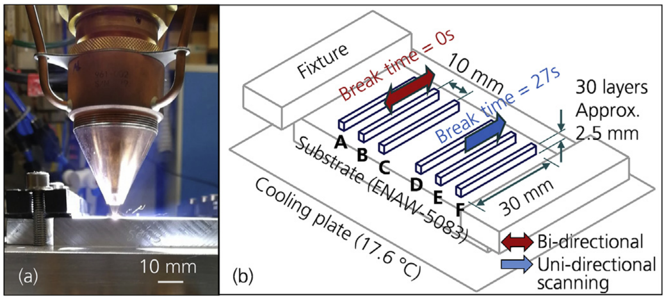

Fig. 1. (a) Experimental set-up, (b) schematic diagram of the experimental layout.

SEM analysis in BSE mode revealed that micron and submicron particles were differently distributed over the cross sections. The specimen (550 W laser power, bi-directionally scanned, aged for 3 h) is shown as one example in Fig. 2(a–d). It can be seen that particles with a number density of 0.057/μm^2 and an average size of 0.112 μm^2 observed in zone I were about 50% fewer and 60% finer than those in zone II and III. Near the bottom in zone IV, the cross sections of the particles with an average size of 0.167 μm^2 were 40% finer than those in zone II and III, but distributed in the most dispersed manner (with a number density of 0.172/μm^2) and covered almost the same total area (area fraction 2.483% in zone II, 3.313% in zone III, 2.864% in zone IV). After etching with NaOH, a boundary was recognized approximately at the upper third position, as indicated by the dashed line in Fig. 2(e). Because a layered structure was recognized only in the part below that boundary, it was considered as the molten pool boundary of the last track.

The layered structure is schematically illustrated in Fig. 3(a). The different zones differed also in terms of the microstructure. As the example in Fig. 3(b) shows, the microstructure in the upper third and near the bottom of the cross section was fine-grained and equiaxed, whereas in the middle it was more coarse and columnar. More details are shown in Fig. 3(c-h): the longest edges of the grains in zone A-B, B-D and D-F were about 3–5 μm, 15–20 μm and 8–10 μm long, respectively. Besides, large columnar grains with the size up to 100 μm were observed below in the connection zone F, as shown in Fig. 3(h).

However, the grain refinement only caused a slight increase of the hardness of the as-casted (namely 0 h artificially aged) specimens. This is shown in the horizontal hardness profiles with insignificant increases of about 10 HV_{10mN} in the upper third part (see Fig. 4(a)① and Fig. 4(b)①-②). A gradual increase of the hardness in the case of the bi-directional specimens produced with 550 W laser power, as shown in Fig. 4(a)①-⑥, was observed only as the ageing duration increased. It was also noted that the ageing response was more significant in the first 3 h (e.g. Fig. 4(a)①-③) than from 3 h to 19 h (e.g. Fig. 4(a)④-⑥), especially as observed on top of the cross section that the hardness was increased from about 110 HV_{10mN} to 170 HV_{10mN} after 3 h and then to 190 HV_{10mN} after 19 h. Similar trends can also be verified in those specimens with 550 W or 600 W laser power and uni-directional scanning, as shown in Fig. 4(b)①-⑥ and Fig. 4(c)⑤-⑥.

In addition, the hardness profiles were also influenced by the applied laser power and scan strategy. As shown in Fig. 4(c), the hardness of the upper part (namely from about 0 to 900 μm) of the specimens (Fig. 4(c)①-④, ⑥) aged for 19 h reached about 200 HV_{10mN}, except for the profile of the specimen (Fig. 4(c)⑤) that reached about 215 HV_{10mN}. However, in the bi-directionally scanned specimens (Fig. 4(c)①-③), as

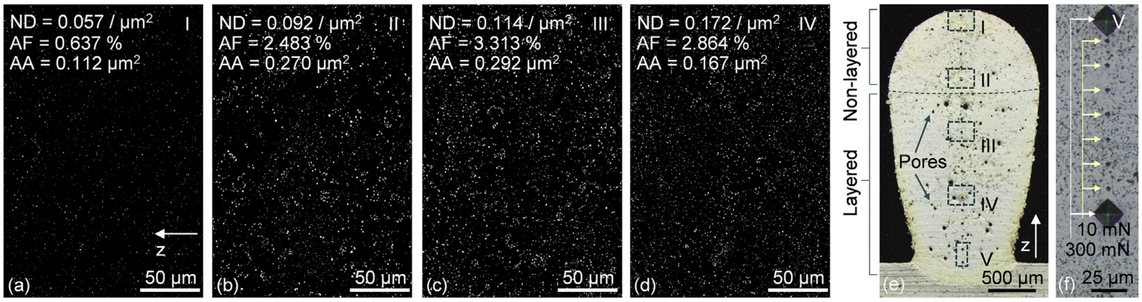

Fig. 2. Binary processed BSE-images of phases in field (a) I, (b) II, (c) III and (d) IV of the polished but non-etched cross section of the specimen bi-directionally welded with 550 W laser power and aged for 3 h (e) LOM-image of the etched cross section. (f) Magnified LOM-image of the hardness indentations in field V, 10 mN for measuring followed by 300 mN for position marking. (LOM = Light optical microscope; ND = Number density [μm^{-2}]; AF = Area fraction; AS = Average size [μm^2]; z: build direction; resolution of BSE-images = 0.033 μm^2).

the laser power increased from 500 W to 600 W, it was apparent that the hardness in the lower part (namely from about 900 μm to 2700 μm) decreased from about 160 HV_{10mN} to about 150 HV_{10mN} and the turning point (namely where the slope changes) of the profile was shifted from about 800 μm to 1100 μm. The situation was different in the uni-directionally scanned specimens (Fig. 4(c)④-⑥), where the highest profile appeared in the specimen processed with 550 W laser power (Fig. 4(c)⑤). This means that the improvement of the mechanical properties cannot be achieved solely by decreasing the laser power or changing the scan strategy, but is influenced by various factors.

The turning points of the profiles shown in Fig. 4 correspond to the position of the boundary of the last resolidified molten pool, as shown in Fig. 3(a). The boundary divides the cross-section of each specimen in two parts, as shown in Fig. 2(a)-(d), in which bright, micrometer-sized, cuboidal-shaped particles are distributed differently. Particles with this size and shape in Al-Mg-Sc-Zr alloys are generally identified as primary $Al_3(Sc,Zr)$ precipitates [2,9,29]. It was found by the EDX-analysis that the average Sc-content in the entire area (detected with plane scan) of zone II and IV (shown in Fig. 2) was found about 0.1 wt.% higher than in zone I, as shown in Table 1. However, in zone I, the mean value of the Sc-content measured (detected with point analysis, Table 1) in the dark area surrounding the particles shown in Fig. 2 was about 0.1–0.2 wt.% higher than in zone II and IV. In addition, the particles in zone II and IV were detected as Sc- and Zr-rich due to the respective content of more than 10 wt.%. It is thus considered that the bright particles detected in this work were primary $Al_3(Sc,Zr)$ precipitates due to the size, shape and composition. Since the total amount of the elemental Sc was fixed, the difference between the Sc-contents detected with point analysis implies that the fraction of the elemental Sc kept in the α-Al matrix (namely the dark area) was higher in the top of the last track (zone I). It is noted that the increasing elemental Sc kept in the matrix promotes secondary precipitation and thus adds to precipitation hardening [9,13]. It is therefore considered that the more obvious ageing response in the upper third, as shown in Fig. 4, was caused by more dispersed and dissolved Sc and Zr elements, as shown in Fig. 2, which were kept in the matrix after the deposition and precipitated during the ageing process.

The grain refinement effect starts to appear in Al-Mg-Sc alloys with a Sc content of approx. 0.4 wt.% [2] and can be further enhanced with an elevated Sc content [3,29]. The need of Sc can be minimized, if Zr is added, as observed in an Al-0.25Sc-0.25Zr (wt.%) alloy [1]. The temperature range, in primary Al_3Sc phases precipitate, is enlarged by additional supplementation of Sc beyond the eutectic value, but can also be suppressed with a high solidification rate [9] that more Sc can be kept in matrix for the secondary precipitation [13]. The ageing temperature applied in this work was selected approximately for the time minima that were found to be at about 300 °C [15] for the transformation of coherent nanometer-sized Al_3Sc precipitates [30] and thus for precipitation hardening [9]. In this study, an apparent hardening was observed after the ageing process instead of through grain refinement alone. The grain refinement was considered to be induced by the primary precipitation [2,3,31,32]. Based on the EDX-analysis shown in Table 1, it is considered that Sc and Zr started to be consumed in the primary $Al_3(Sc,Zr)$ precipitates at the molten pool boundary. The solute in the liquid phase would be transferred to the solidification front [26] and thus as considered be diluted in the molten pool center. The actual liquidus temperature in the molten pool center was therefore lower than the theoretical value. The freezing zone was thus minimized, so that the material would be kept in liquid phase longer and Sc and Zr were thus promoted to be more homogeneously distributed [9]. As the growth of $Al_3(Sc,Zr)$ precipitates is diffusion-controlled [4,30], a homogeneous distribution of the elements would induce a disperse formation of both primary and secondary precipitates. As zone II and IV (Fig. 2(e)) were at the molten pool boundaries remaining after the

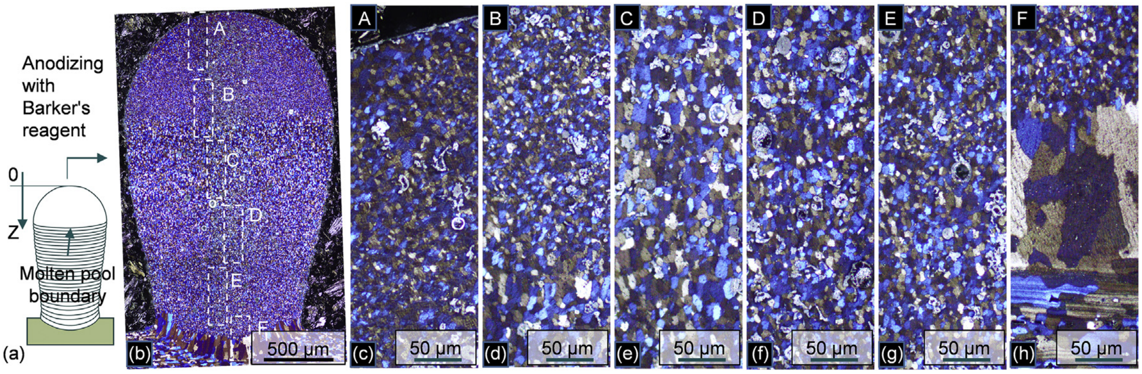

Fig. 3. Schematic illustration of the track overlapping (a). Polarized light microscopy of the cross section of the specimen bi-directionally welded with 550 W laser power, stored at RT and electrolytically etched with Barker's reagent - the overall image (b) and the magnified image of field A-F ((c)–(f). (Z: top down direction).

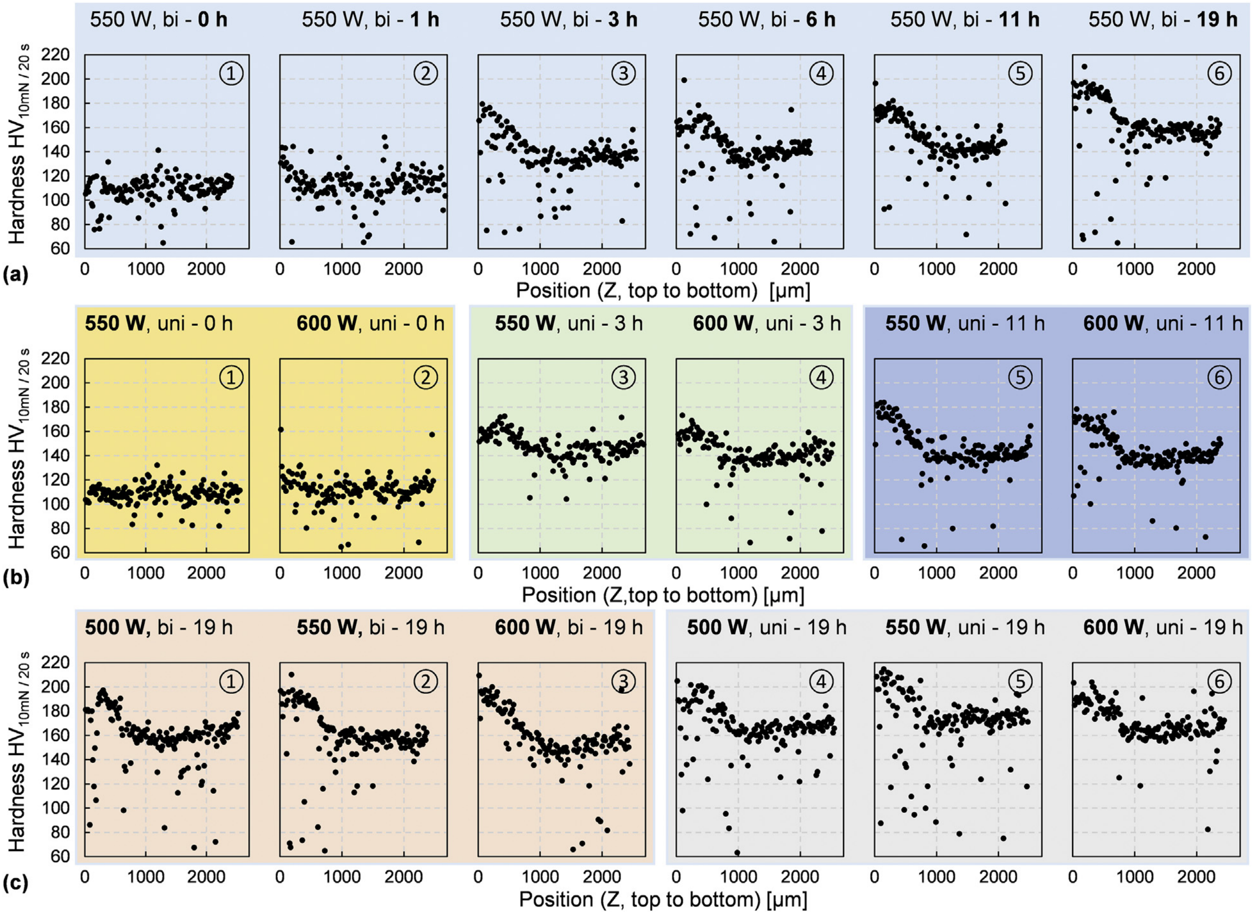

Fig. 4. Hardness profiles sampled top down from the axes of symmetry of the cross sections of the thin-wall specimens: (a) bi-directionally scanned with 550 W laser power and aged for different durations from 0 h to 19 h; (b) uni-directionally processed with laser power of 500 W, 550 W or 600 W and stored at room temperature (aged for 0 h) or aged for 3 h or 11 h; (c) aged for 19 h but differently processed. Designation "xx, yy - zz": "xx" - the laser power reaching on workpieces, "yy" - the scan strategy (bi: bi-directional without a break time; uni: uni-directional with 27 s break time), "zz" - the artificial ageing duration in oven at 300 °C. The low hardness runaway values were occasionally sampled on pores. The hardness values (4–8 points in each profile) lower than 60 HV_{10mN} were filtered out.

Table 1

Relative element distribution measured by EDX-analysis in zone I, II and IV (as marked in Fig. 2(e)) of the cross section of the specimen bi-directionally welded with 550 W laser power and aged for 3 h (M: plane scan mode of the whole area. P: point analysis mode of the dark area, 40% trimmed mean of n = 10 sampling. Rest: Si, Ar, Fe, Zr, Ag. Normalized wt. % by eliminating C and O. Notice the relative significance of the values. The second digit after the decimal point is for reference only).

Mode	Zone	Al	Mg	Mn	Sc	Rest
M	I	94.02	3.91	0.51	0.68	bal.
M	II	94.06	3.90	0.59	0.78	bal.
M	IV	93.76	3.69	0.60	0.76	bal.
P	I	94.11	3.94	0.46	0.68	bal.
P	II	94.78	3.44	0.49	0.47	bal.
P	IV	94.37	3.78	0.45	0.58	bal.

overlapping of tracks and zone I was the molten pool center of the last track (Fig. 2(e)), the average Sc-contents detected (M-mode) in the whole area of zone II and IV was therefore higher than of zone I, as shown Table 1.

The thermal condition of the material deposition changes as a specimen is being built up [27]. This is proven especially for the bi-directionally scanned specimens, where it was observed that as the laser power increased, the turning points that indicate the position of the molten pool boundaries of the last tracks were shifted lower (Fig. 4(c)①-③). The growing grain sizes from bottom to top inside the layered part (Fig. 3(b)E-C) are considered to be caused by the increasing heat accumulation. The dilution of the powder material with the substrate, which does not contain Sc and Zr, resulted in formation of coarse columnar grains at the bottom (Fig. 3(b)F). Considering that during the process the material at the molten pool boundary was in a mushy state [26] and the cooling rate of the LMD-process might be too low to achieve a high supersaturation, the primary $Al_3(Sc,Zr)$ precipitates could easily grow at the expense of the dissolved Sc and Zr [20], so that less secondary precipitation occurred leading to a low hardness profile in the layered zone.

In summary, Al-4.55Mg-0.51Mn-0.65Sc-0.30Zr alloy was processed in LMD process in this study. Equiaxed 3–5 µm and 8–10 µm sized grains were observed in the last track and near the bottom, respectively, while columnar 15–20 µm sized grains were observed in the middle of the cross sections. The difference in grain size corresponded to only about 10 HV_{10mN} difference in hardness. A hardness increase of up to 80 HV_{10mN} was observed after ageing for 19 h in the last track but not in the layered zone instead of with the grain refinement alone. This difference was correlated with the formation of particles containing Sc and Zr. The primary precipitates were formed at the expense of rare elements for forming secondary precipitates, which are required for precipitation hardening. However, the cooling rate in LMD appeared to be too low to suppress the mushy state and thus to realize a dispersed nucleation and a weak growth of primary precipitates. Changing parameters has not been found to be a proper approach to achieve precipitation hardening and grain refinement in thin walls.

Acknowledgement

This work was supported by the NSFC-DFG Sino-German Research Project (Grant No. GZ 1217).

References

[1] A.F. Norman, P.B. Prangnell, R.S. McEwen, Acta Mater. 46 (1998) 5715–5732.

[2] S'a Zhou, Z. Zhang, M. Li, D. Pan, H. Su, X. Du, et al., Mater. Des. 90 (2016) 1077–1084.

[3] W.G. Zhang, Y.C. Ye, L.J. He, P.J. Li, X. Feng, L.S. Novikov, Mater. Sci. Eng. A 578 (2013) 35–45.

[4] E. Clouet, L. Laé, T. Epicier, W. Lefebvre, M. Nastar, A. Deschamps, Nat. Mater. 5 (2006) 482–488.

[5] J.H. Martin, B.D. Yahata, J.M. Hundley, J.A. Mayer, T.A. Schaedler, T.M. Pollock, Nature 549 (2017) 365–369.

[6] J.R. Croteau, S. Griffiths, M.D. Rossell, C. Leinenbach, C. Kenel, V. Jansen, et al., Acta Mater. 153 (2018) 35–44.

[7] A.B. Spierings, K. Dawson, K. Kern, F. Palm, K. Wegener, Mater. Sci. Eng. A 701 (2017) 264–273.

[8] Y. Buranova, V. Kulitskiy, M. Peterlechner, A. Mogucheva, R. Kaibyshev, S.V. Divinski, et al., Acta Mater. 124 (2017) 210–224.

[9] K.L. Kendig, D.B. Miracle, Acta Mater. 50 (2002) 4165–4175.

[10] A. Gasser, G. Backes, I. Kelbassa, A. Weisheit, K. Wissenbach, LTJ 7 (2010) 58–63.

[11] W. Xu, M. Brandt, S. Sun, J. Elambasseril, Q. Liu, K. Latham, et al., Acta Mater. 85 (2015) 74–84.

[12] P. Kürnsteiner, M.B. Wilms, A. Weisheit, P. Barriobero-Vila, E.A. Jägle, D. Raabe, Acta Mater. 129 (2017) 52–60.

[13] J. Taendl, A. Orthacker, H. Amenitsch, G. Kothleitner, C. Poletti, Acta Mater. 117 (2016) 43–50.

[14] E.A. Jägle, Z. Sheng, L. Wu, L. Lu, J. Risse, A. Weisheit, et al., JOM 68 (2016) 943–949.

[15] J. Røyset, N. Ryum, Mater. Sci. Eng. A 396 (2005) 409–422.

[16] D. Tomus, M. Qian, C.A. Brice, B.C. Muddle, Scripta Mater. 63 (2010) 151–154.

[17] P. Yu, M. Yan, D. Tomus, C.A. Brice, C.J. Bettles, B. Muddle, et al., Mater. Char. (2018), https://www.sciencedirect.com/science/article/pii/S1044580317323513.

[18] B. Zheng, Y. Zhou, J.E. Smugeresky, J.M. Schoenung, E.J. Lavernia, Metall. Mater. Trans. 39 (2008) 2228–2236.

[19] B. Zheng, Y. Zhou, J.E. Smugeresky, J.M. Schoenung, E.J. Lavernia, Metall. Mater. Trans. 39 (2008) 2237–2245.

[20] Y. Shi, P. Rometsch, K. Yang, F. Palm, X. Wu, Mater. Lett. 196 (2017) 347–350.

[21] A.B. Spierings, K. Dawson, T. Heeling, P.J. Uggowitzer, R. Schäublin, F. Palm, et al., Mater. Des. 115 (2017) 52–63.

[22] A.B. Spierings, K. Dawson, P.J. Uggowitzer, K. Wegener, Mater. Des. 140 (2018) 134–143.

[23] K.V. Yang, Y. Shi, F. Palm, X. Wu, P. Rometsch, Scripta Mater. 145 (2018) 113–117.

[24] A.B. Spierings, K. Dawson, M. Voegtlin, F. Palm, P.J. Uggowitzer, CIRP Annals 65 (2016) 213–216.

[25] A.B. Spierings, K. Dawson, P. Dumitraschkewitz, S. Pogatscher, K. Wegener, Add. Manuf. 20 (2018) 173–181.

[26] H. Zhang, D. Gu, J. Yang, D. Dai, T. Zhao, C. Hong, et al., Add. Manuf. 23 (2018) 1–12.

[27] P.A. Rometsch, H. Zhong, K.M. Nairn, T. Jarvis, X. Wu, Scripta Mater. 87 (2014) 13–16.

[28] M. Awd, J. Tenkamp, M. Hirtler, S. Siddique, M. Bambach, F. Walther, Materials 11 (2017) (Basel, Switzerland).

[29] S. Costa, H. Puga, J. Barbosa, A.M.P. Pinto, Mater. Des. 42 (2012) 347–352.

[30] E.A. Marquis, D.N. Seidman, Acta Mater. 49 (2001) 1909–1919.

[31] S'a Zhou, Z. Zhang, M. Li, D. Pan, H. Su, X. Du, et al., Mater. Char. 118 (2016) 85–91.

[32] Z. Yin, Q. Pan, Y. Zhang, F. Jiang, Mater. Sci. Eng. A 280 (2000) 151–155.